Research & Reviews: Journal of Statistics and Mathematical Sciences

Two-Dimensional Analytical Model and Control of Linear Induction Motor

Ehsan Shirzad*

Department of Electrical and Electronics Engineering, University of Bojnord, Bojnord, Iran

Research Article

Received: 03-Jan-2024, Manuscript No. JSMS-24-124329; **Editor assigned:** 05-Jan-2024, Pre QC No. JSMS-24-124329 (PQ); **Reviewed:** 19-Jan-2024, QC No. JSMS-24-124329; **Revised:** 26-Jan-2024, Manuscript No. JSMS-24-124329 (R); **Published:** 02-Feb-2024, DOI: 10.4172/ RRJ Stats Math Sci. 10.01.001

***For Correspondence:** Ehsan Shirzad, Department of Electrical and Electronics Engineering, University of Bojnord, Bojnord, Iran

E-mail: **Ehsan_Shirzad_72@yahoo.com**

Citation: Shirzad E. Two-Dimensional Analytical Model and Control of Linear Induction Motor. RRJ Stats Math Sci.2024.10.001.

ABSTRACT

Through electromagnetic forces, Linear Electric (Electromagnetic) Machines (LEMs) can directly convert electrical energy into linear mechanical kinetic energy (*vice versa*). Linear motion is especially common in industry. LEM was developed in his 19th century, but did not become widely used in industry until 1960 because it required power electronics (no mechanical transmission) for control. However, LEMs require power electronics for linear position, speed, and/or force control to achieve better performance than rotary electric motors with mechanical transmissions. After 1960, LEM continued to improve. The lift and drive forces of a two-phase Linear Induction Motor (LIM) are controlled by varying the phase angle between the two phases. In this article, we derive the magnetic flux density, secondary current density, and propulsion and levitation force densities in the air gap. The mean force equation is derived by summing the force density over a quadratic length using two-dimensional magnetic field analysis and is used to simulate the performance of a linear induction motor. We investigate the effect of changing the phase angle on the secondary current density, perpendicular magnetic flux density component, and tangential magnetic flux density component. Furthermore, these phase-shifting effects are extended to include his two components of force (levitation and propulsion). Calculations are performed using MATLAB programs and displayed graphically.

Keywords: Density; Magnetic flux; Magnets; Electric

LIST OF ABBREVIATIONS

MAGLEV-Magnetically Levitated; LEM-linear electric (electromagnetic) machines; LIMs-linear induction motors; PMs-Permeant Magnets

INTRODUCTION

Depending on the method used for magnetic field analysis, the electrical stress on a magnetic circuit is usually expressed in the form of a Fourier series or Fourier integral. It is clear that determining the motor force requires knowledge of the excitation secondary current density and the air gap magnetic flux density components. The current density and magnetic flux density components are fully determined by solving the magnetic vector potential equations and applying boundary conditions. It must be expressed in a format suitable for analysis. The use of a Linear Induction Motor (LIM) is considered an effective approach to achieve a smooth drive. LIM operation does not require the use of Permanent Magnets (PM), thus avoiding the increased weight and cost of the MAGLEV system. The available publications on LIM are very diverse, and most are written for a specific LIM with specific operations. It is reasonable to believe that a two-dimensional analysis will yield better results than his one-dimensional theory when calculating the performance of a motor. Analyze LIM efficiency using a maglev train drive system. This system has the highest energy consumption. This is because the efficiency of LIM increases as the slip frequency decreases. In this article, the components of secondary current density and air gap magnetic flux density are used to study the performance and characteristics of levitation and propulsion forces. The analysis is performed by his two-dimensional application of the field system using two models, with and without iron base [1-10].

Two-dimensional model with back-iron

In this work, the study is interested in two-dimensional field analysis because the air gap field has both y and x flux components. If x flow component is present, a non-constant in the y direction is required to satisfy the condition

Div $\vec{B} = 0$.

Variation of the y-component of the air gap field along the air gap length including a conductive secondary sheet metal line. In addition to current shift phenomena in secondary leaves. The two-dimensional magnetic field analysis is performed using a magnetic vector potential that is a rotation of B. This allows us to consider the effects of physical air gaps and finite magnetic permeability and conductivity in different regions in the y direction. A model for two-dimensional field analysis of a steel-based machine is shown in Figure 1. The coordinate axes are selected as shown.

Figure 1. Two-Regions model for the two-dimensional analysis.

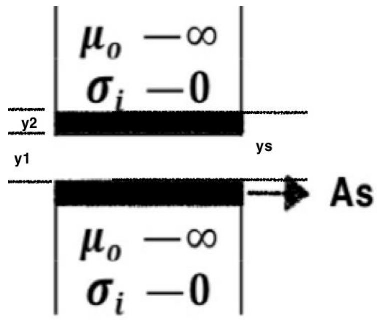

Region 1: $o \le y \le y1$, is the air gap region between the stator and the secondary.

Region 2: $y1 \le= y \le ys$ the secondary conductive layer $ys = y1 + tc$ In this idealized model, the effects of hysteresis and saturation are also ignored, and the stator has infinite permeability and conductivity will be zero.

In this model, a smooth surface stator with continuous current plates and an electric stator load (As) is used instead of a slotted stator.

$$A_s(x,t) = \mathrm{Re}\sum_m \underline{A}_{sm} ej^{(wt-ax)} \quad \text{........ (1)}$$

The current flowing in the z direction corresponds to the stator current. It is only assumed that the secondary current is still flowing in the axial z direction. As a result, the magnetic flux density B and the magnetic field strength H both have x and y components. The electromagnetic theory approach is based on Maxwell's field equations for an isotropic medium.

$$\text{Cur 1}\,\vec{H} = \vec{J},\quad \text{Cur 1}\,\vec{E} = \frac{\overrightarrow{\partial B}}{\partial t} + \text{Cur 1}\,(\vec{v}X\vec{B}) \quad \text{......... (2a, b)}$$

They are complemented by the continuity conditions

$$\text{Div}\,\vec{J} = 0,\ \text{div}\ \vec{B} = 0 \quad \text{...... (3a, b)}$$

and the relation between the magnetic field intensity and flux density.

$$\vec{B} = \mu\vec{H} \quad \text{....... (3c)}$$

The current density is obtained by

$$\vec{J} = \sigma\vec{E} \quad \text{........... (4)}$$

The magnetic vector potential $\vec{V}$ is defined by

$$\vec{B} = Cur1\overrightarrow{V} \quad \text{............. (5a)}$$

with the complementary condition

$$\text{div}\,\vec{V} = 0 \quad \text{.................. (5b)}$$

and the magnetic Reynold's number r is

$$r = W\mu_0\frac{\sigma}{.} \quad \text{............ (5c)}$$

In the air-gap region, with zero conductivity

$$\frac{\partial^2 V_{Z1}}{\partial y^2} - a^2\underline{V}_{\,Z}1(\text{y}) = 0 \quad \text{............... (6)}$$

By resolving the differential equations (5C) and (6) in accordance with the problem's geometry, the magnetic vector potentials are derived. The complex amplitudes of the vector are obtained from the solution of these differential equations.

$$\underline{V}_Z 2 = C_{2.}e^{ky} + D_2.e^{-ky} \quad \text{................ (7)}$$

$$\underline{V}_Z 1 = C_{1.}e^{ay} + D_1.e^{-ay} \quad \text{...... (8)}$$

Where C and D are the integration constants which will be determined by applyingthe boundary conditions.

The boundary conditions

Applying the following boundary conditions will allow us to evaluate the unknown integration constants C and D:

The tangential component of the field intensity H_x is continuous across each interregional boundrary.

$$H_X = \frac{1}{\mu}\frac{\partial V_Z}{\partial y} \quad \text{........ (9a)}$$

We have, at the boundary between regions n and n + 1,

$$\frac{1}{\mu}\frac{\partial V_Z}{\partial y} = \frac{1}{\mu+1}\frac{\partial V_Z+1}{\partial y} \quad \text{......... (9b)}$$

At the first air gap stator boundary, the condition becomes modified by introducing the exciting stator electric loading

$$\frac{1}{\mu}\frac{\partial V_{Z1}}{\partial y}|_{y=0} = A_{s\,,} \quad \text{......... (10a)}$$

Since μii tends to infinity.

At the secondary air gap-core, boundary yields.

$$\frac{1}{\mu}\frac{\partial V_{Z2}}{\partial y}|_{y=ys} = 0 \quad \text{....... (10b)}$$

The same condition is to be applied at the air gap-secondary boundaries yielding,

$$\frac{1}{\mu}\frac{\partial V_{Z1}}{\partial y}|_{y=y1} = \frac{1}{\mu}\frac{\partial V_{Z2}}{\partial y}|_{y=}y1 \text{ ...... (10c)}$$

The continuity of the vector potential (Vzn = Vzn +1) is implied by the fact that the normalcomponent of the flux density By is continuous across each interregional boundary.

When the stipulation is used at the secondary-air gap border,

$$V_{Z1}|_{y=y1} = V_{Z2}|_{y=y1} \text{ .... (10d)}$$

To fully determine the integration constants P and Q, the conditions in equations (10a-d) must be met. Hence, the vector potential for the two regions and the flux density components can be completely obtained.

Applications of the boundary conditions gives the four integration constants of the two regions. Thus, the flux density components due to the stator electric loading in the differentmachine regions are

$$B_{X1} = a(C_1e^{ay} - D_1e^{-ay}) \text{ ...... (11a)}$$

$$B_{y1} = j\, a(C_1e^{ay} - D_1e^{-ay}) \text{ ...... (11b)}$$

$$B_{X2} = k\,(C_2e^{ky} - D_2e^{-ky}) \text{ .... (11c)}$$

$$B_{y2} = j\, a\,(C_2e^{ky} - D_2e^{-ky}) \text{ .... (11d)}$$

Simulation results of phase angle control for LIM with iron backing

The driven force is function of (By, Jz) and the levitation force is function of (Bx,Jz), as theamplitudes of :- Fy=Bx.Jz and Fx=By.Jz.

From the following graphs Figure 2. (Levitation Force with iron backing with the speed v [m/s]) and Figure 3 (drive force with iron backing with the speed v [m/s]) the relations between the flux density in the x-direction and speed is illustrated decreasing the flux density with increasing the speed.

Figure 2. Levitation force with iron backing with the speed v [m/s].

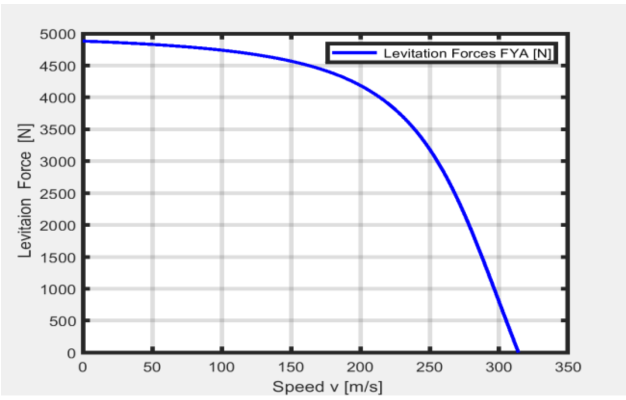

Figure 3. Drive force with iron backing with the speed v [m/s].

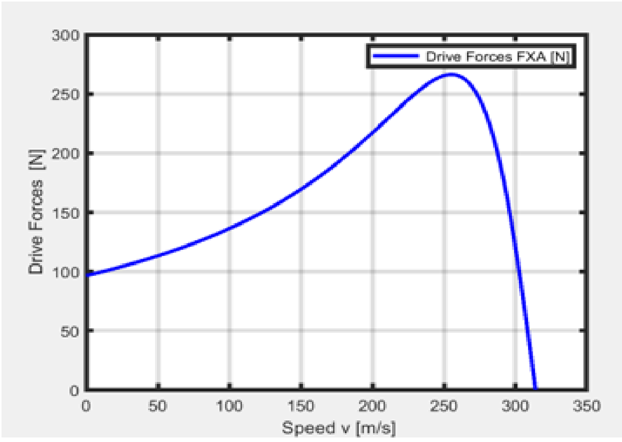

The Two-Dimensional field analysis without iron backing

The three regions of the model in Figure.4 are defined as follows:

Region 1: $0 \leq y \leq y_{2,}$ is the first air-gap between the external stator and the secondary sheet.

Region 2: $y_2 \leq y \leq (y_2 + y_r)$, is the secondary sheet conducting layer.

Region 3: $(y_2 + y_r) \leq y \leq y_{s,}$ the second air-gap between the secondary sheet layer andthe iron core.

Figure 4. Two-dimensional analysis without iron backing (three regions models).

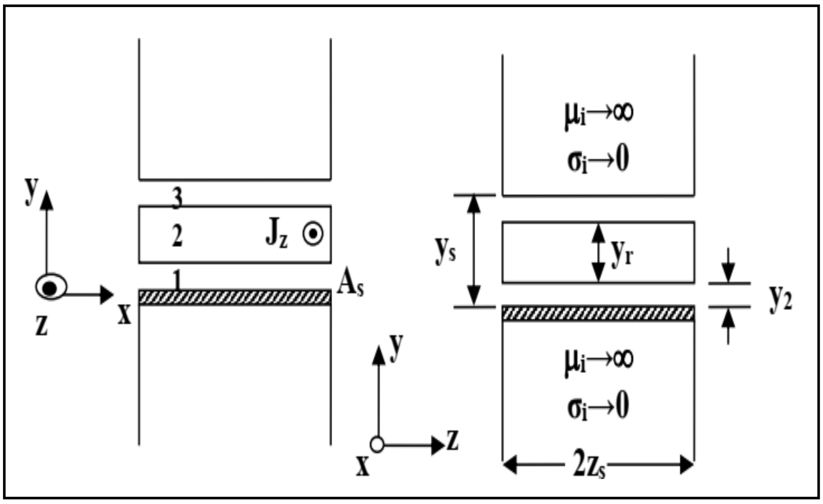

Simulation of phase angle control for LIM without iron backing

The following graphs (Figures 5-9) show many parameters (Current Density, Levitation Flux Density (Bx), Drive Flux Density (Bx) , Levitation Force (N) and Drive Force (N)) with the speed v [m/s]. as clear how speed and the flux density in the x-direction relate to one another, with speed decreasing the flux density.

Figure 5. Current density J Z with the speed v [m/s].

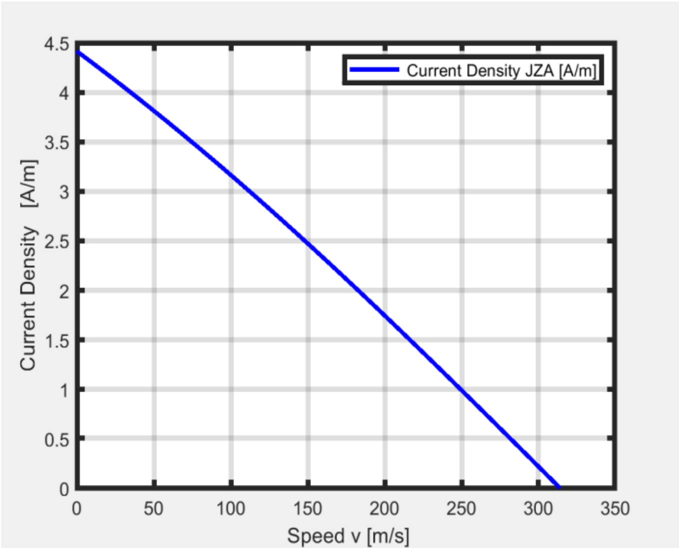

Figure 6. Levitation flux density (bx) with the speed v [m/s].

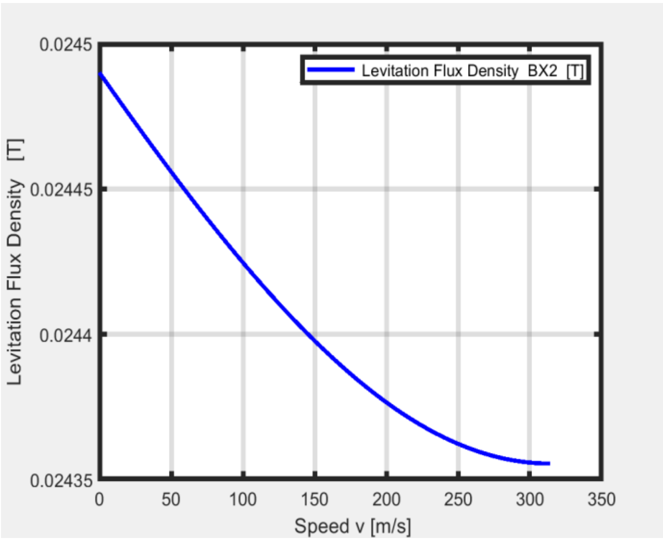

Figure 7. Drive flux density (bx) and the speed v [m/s].

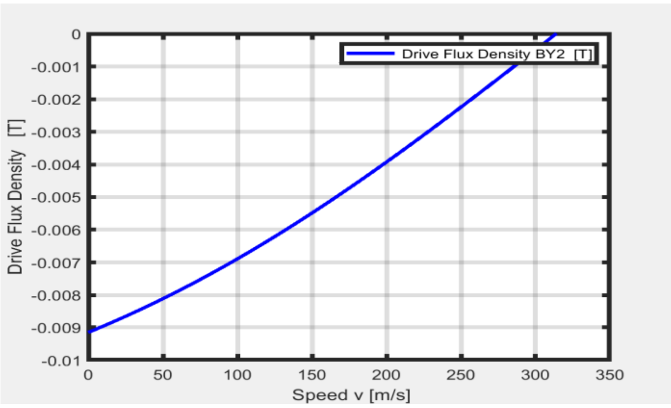

Figure 8. Levitation force (N) and the speed v [m/s].

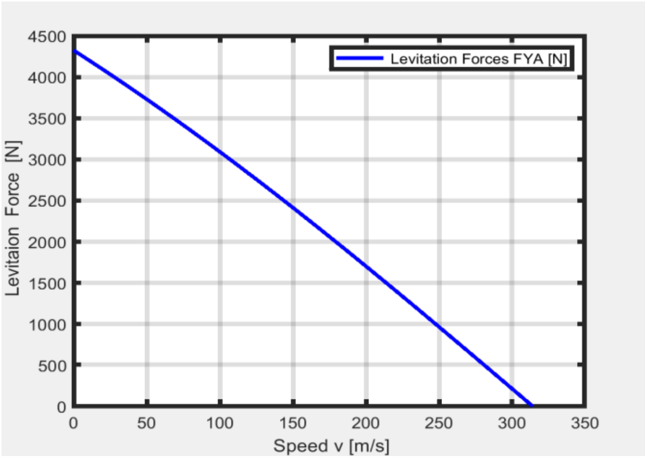

Figure 9. Drive force (N) and the speed v [m/s].

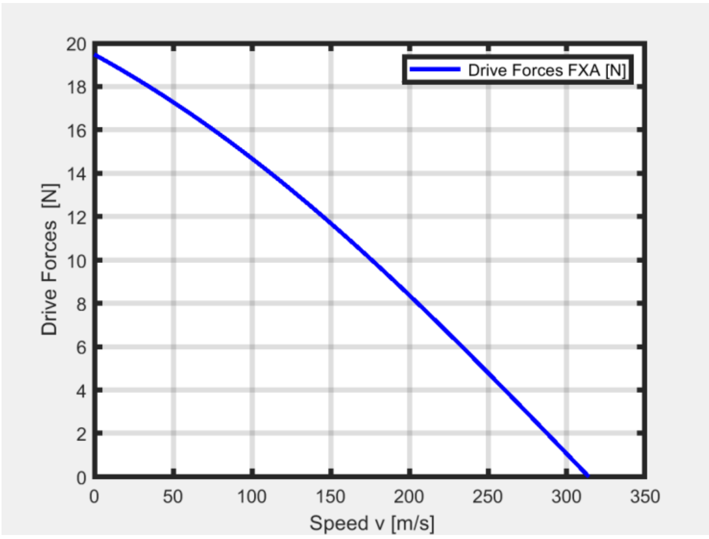

Comparison between forces with backing and without iron backing

As illustrated below in Figures 10-13, the relations between (Drive and Levitation forces with iron backing and without iron backing in different cases)

Figure 10. Drive and levitation forces without iron backing with the speed m [m/s].

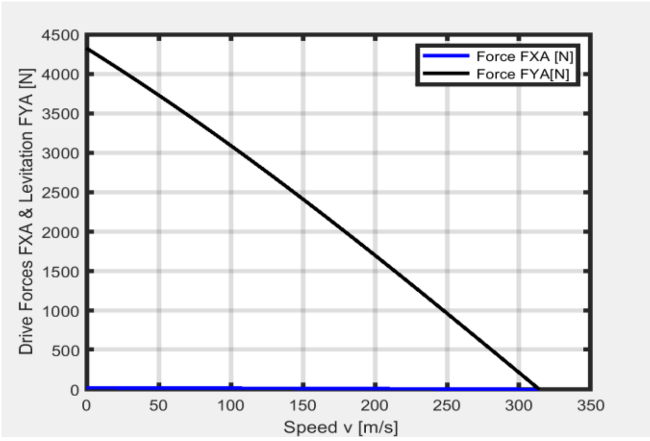

Figure 11. Drive forces with and without iron backing with the speed m [m/s].

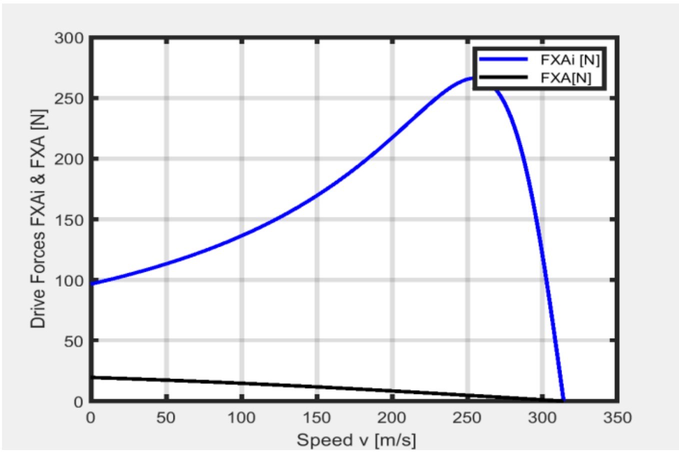

Figure 12. Levitation force with and without iron backing with the speed v [m/s].

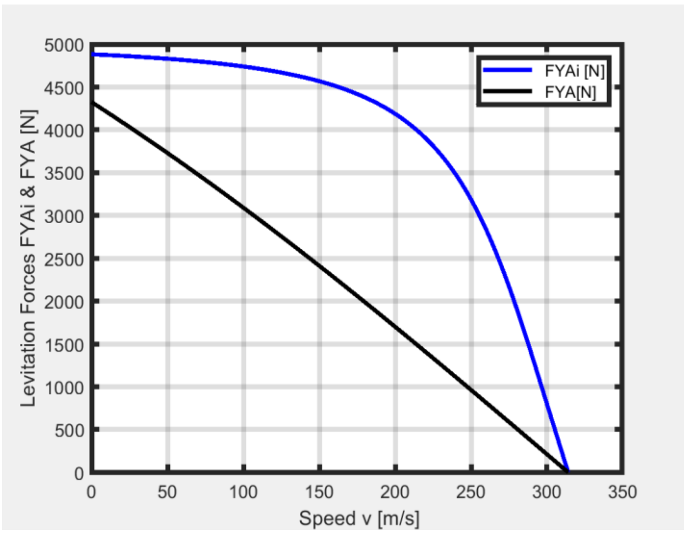

Figure 13. Drive force and levitation force with iron backing with the speed m[m/s].

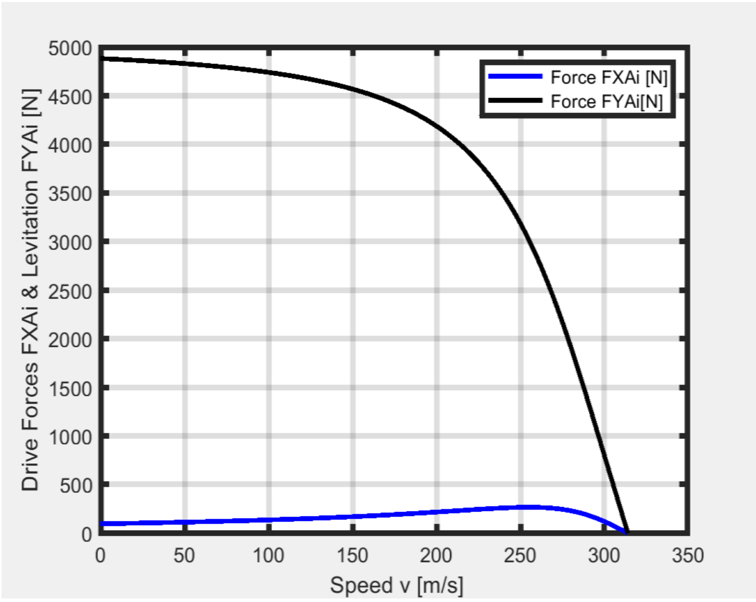

Control with IGBT

Using the phase angle value between the two phases voltage source to control the outputcharacteristics of the motor:

Figure 14. Phase angle control circuit diagram of two-phase induction motor [11-20].

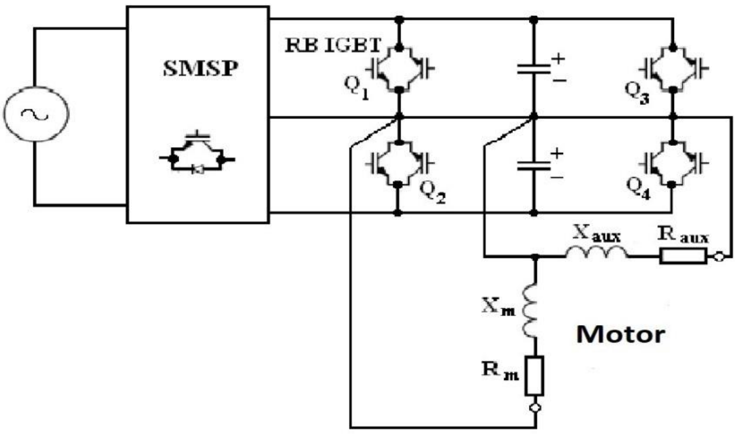

For the phase angle control at four values of this angle using the iron backing case in somecontrol cases.

As in the following figures (Figures 15-18).

Figure 15. Drive force at different values of phase angle between the two phases with the linear speed [m/s] considered the control angles are (0º, 30º, 45º and 90º).

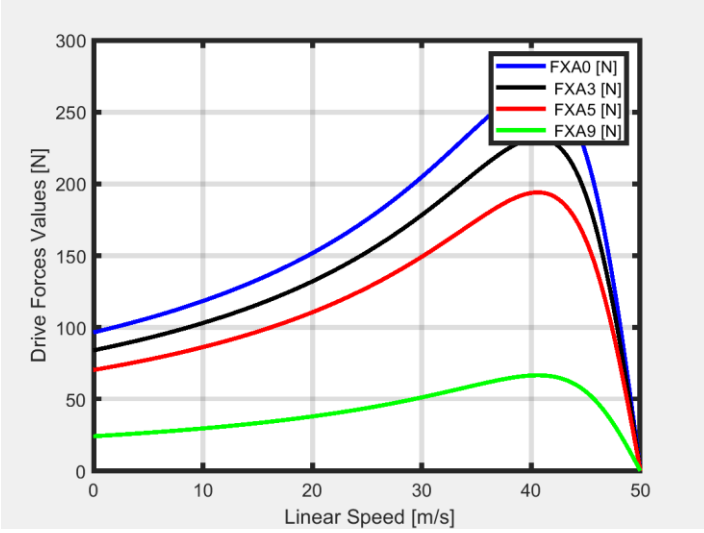

Figure 16. Levitation force at different values of phase angle between the two phases with the linear speed [m/s] Considered the control angles are (0º, 30º, 45º and 90º).

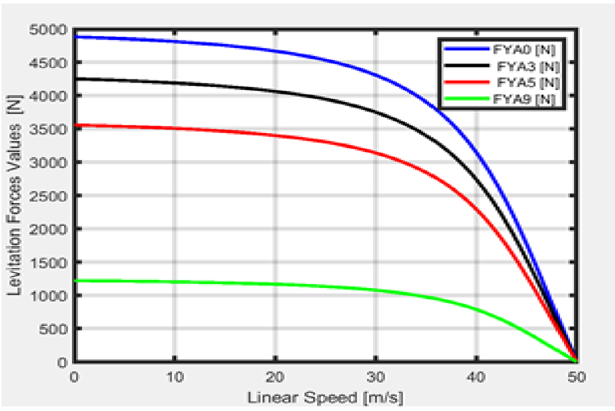

Figure 17. Average levitation force Density [N/m²] at different values of phase angle between the two phases with the Linear Speed [m/s] considered the control angles are (0º, 30º, 45º and 90º).

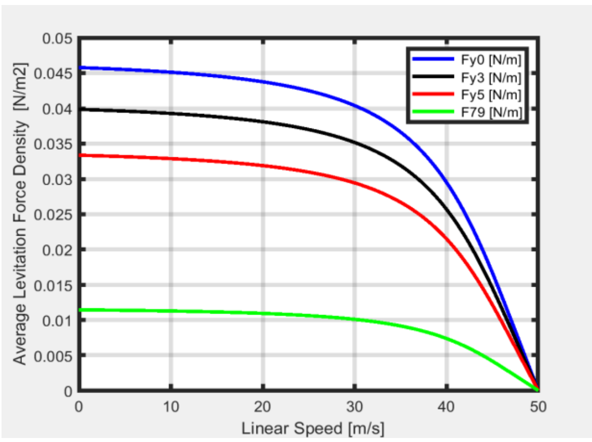

Figure 18. Average Drive force density [N/m²] at different values of phase angle between the two phases with the linear Speed [m/s] considered the control angles are (0°, 30°, 45° and 90°).

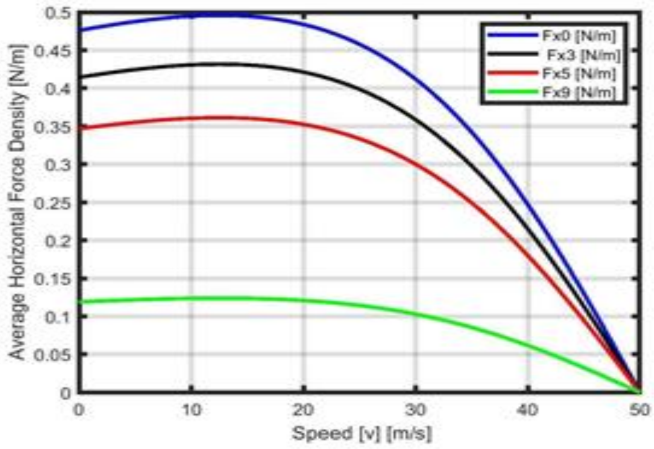

RESULTS AND DISCUSSION

From all the previous figures, a large force value is obtained when the control angle is 0° (the phase angle between the two phases is 90°), so the phase angle is used to control the propulsion and levitation forces and can control the values of these forces at different values of controlled angles [21-30]. The magnetic field analysis in Cartesian coordinates is performed based on a two-domain model starting from Maxwell's magnetic field equations. Two models were selected.

- With secondary iron support (with internal air gap area and conductive secondary area).
- No secondary iron-back (with inner air gap region, outer air gap region, and conductive secondary region).

From the point of view of electromagnetic theory, this approach is based on Maxwell's field equations for an isotropic medium moving with velocity $\vec{v}$, to obtain differential equations describing the vector potential in different regions. Solve the field equations using boundary conditions for each case. The unknown integration constants C and D are evaluated by applying appropriate boundary conditions. The air gap flux density and secondary current density components due to the stator electrical load are expressed using two-dimensional analysis. Air gap flux density and secondary current density distributions can be easily calculated and graphed using a variety of models. These calculations are done using mechanical design data. The normalized components of redial by and tangential flux density Bx are plotted against engine speed. Models with iron supports on the stator and secondary of the motor have a higher radial flux density than models without iron supports. The secondary current density has a maximum value at standstill, and as the speed increases, the secondary current density decreases. This is the main effect of armature reaction force. Two components of force characteristics (propulsive force and levitation force) are determined and examined for different models. Demonstrate phase shift control by varying the phase shift angle from 0 to 90°, and compare its characteristics [31-43].

CONCLUSION

In this paper, we have extensively examined the functionality of Linear Induction Motors (LIM) featuring back iron components. Our focus has been on elucidating a comprehensive two-dimensional model to effectively compute both force and flux density within the system. This meticulous model stands as a reliable alternative to the conventional finite element method, offering enhanced accuracy and efficiency in calculations pertaining to LIMs. By delving into the intricacies of LIMs with back iron, the aim is to provide analytical toolset for optimizing motor performance and design. Through rigorous analysis and validation, it establishes the viability and efficacy of this two-dimensional model, paving the way for its practical implementation in diverse applications.

REFERENCES

1. Vladimir Kuptsov, et al. Combined propulsion and levitation control for maglev/hyperloop systems utilizing asymmetric double-sided linear induction motors. Mach. 2022;10:131.
2. AA. Kuijpers, et al. Force analysis of linear induction motor for magnetic levitation system. EPE-PEMC. 2010.
3. Yamamura S, et al. Theories of the linear, Induction motor and compensated linearinduction Motor. IEEE. 1972;91:1700-1710.
4. Hyunuk Seo, et al. A study on efficiency of magnetic levitation trains using linear induction motor by slip pattern. Energy Convers. Congr. Expo. 2019.
5. Popescue M, et al. Analytical prediction of electromagnetic torque in single phase *and two phase of ac motors*. Energy Convers. Congr. Expo. 2004.
6. Theraja B. L, et al. A textbook of electrical technology. 2003;1367-1977.
7. JH Sung, et al. A new approach to vector control for a linear induction motor considering end effects. Energy Convers. Congr. Expo. 1999;4:2284–2289.
8. Rakesh P. AC induction motor fundamentals. Micro Techno. Inc. 2003;3-6.
9. Storey J. How real electric motors work. 2011.
10. Sen P. C. *P*rinciples of electric machines and power electronics. 1997;373-392.
11. A K Rathore et al. Decoupled control of attraction force and propulsion force in linear induction motor drive. IEEE Int. Conf. Ind. Technol. 2003;1:524–529.
12. Oliveira, et al. Vector control for linear induction motor. IEEE Int. Conf. Ind. Technol. 2003; 1:518–523.
13. Agarwal R. K. Principle of electrical machine design 4thedition. 2000;366-381.
14. Ryszard Palka, et al. Linear induction motors in transportation. Elec Eng. 2021.
15. Zhendong Liu, et al. Technology and development of maglev and hyperloop systems. 2022;01:14.
16. Anton J.D. Verdel. Decoupled control of thrust and normal forces of linear induction motor for a novel magnetically levitated system. 2007.
17. Hirahara, et al. A method to calculate the performance of linear induction motors using simple two-phase model. 2021.
18. A K Rathore, et al. Simulation of secondary flux oriented control oflinear induction motor considering attraction force & trans- verse edge effect. IEEE Power Electron. Lett. 2004;158–163.
19. G Kang , et al. Field-oriented control scheme for linear induction motor with the end effect. IEE Proc. Electr. Power Appl. vol. 2005;152:1565–1572.
20. Oliveira, et al. Dynamic model for linear induction motor. IEEE Int. Conf. Ind. Technol. 2003;1:478–482.
21. N T Morizane, et al. Simultaneous control of propulsion and levitation of linear induction motor in a novel maglev system. 2000;1:127–131.
22. T Yoshida. Decoupled-control method of normal and thrust forces in linear induction motor for maglev vehicle marine-express me01. IEEE Inter Conf Elec Mac. 1999;369–371:9-12 May.
23. T K Yoshida, et al. Influence of instantaneous end effects on attractive levitation force at standstill of combined-levitation-and- propulsion slim. IEEE.
24. Sixth international conference on electrical machines and systems. 2003;1:187–190.
25. S Yamamura. Theory of linear induction motors. 1972.
26. J F Gieras. Linear induction drives. 1994.
27. G J F Gieras et al. Performance calculation for single- sided linear induction motors with a double-layer reaction

rail under constant current excitation. 1986;22:54-62.
28. I Boldea, et al. Linear motion electromagnetic systems. 1985.
29. I Boldea, et al. A complete equivalent circuit of a linear induction motorwith sheet secondary. IEEE. 1988;24:639-654.
30. F Sahin. Linear induction motor design overview. Tech. Rep. 2005.
31. G J F Gieras, et al. Performance calculation for single- sided linear induction motors with a solid steel reaction plate under constant current excitation. IEEE Proce, 1985;132:185–194.
32. I Takahashi, et al. Decoupling control of thrust and attractive force of a LIM using a space vector control inverter. IEEE Trans on Indu Appl. 1993;29:161–167.
33. ION BOLDEA. Linear Electric Machines, Drives, and MAGLEVs Handbook. 2012.
34. E Shirzad. Sub-Region model for flux-switching permanent magnet machine with outer rotor and inner rotor distinctly to calculate cogging torque, electromagnetic torque and inductance (self and mutual). 2023.
35. E Shirzad. Optimized design by genetic algorithm for flux switching brushless permanent magnet machines with two ports from perspective of losses. 2023.
36. Shirzad E. UPS design without inverter to power ISP servers. 2023.
37. Shirzad E. Calculation of flux density in air-gap for reluctance motor with two ports (double-stator, double- rotor) by Fourier Series. 2023.
38. Shirzad E. Solving partial derivation equations in detail in double- rotor flux switching permanent magnet with h-shape stator machines to obtain magnetic flux density. 2023.
39. Shirzad E. Analytical model for double-sided linear permanent magnet inner armature synchronous machine with slot-less stator at on-load in different patterns of magnetization. Elect Engin.2023.
40. Shirzad E, et al. Analytical model for brushless double mechanical port flux- switching permanent magnet Machines. IEEE Trans. Magn. 2021.
41. Shirzad E. Fast-response method for e-core switched-flux permanent-magnet brushless machine with outer rotor to predict distribution of flux density at no-load. 2022.
42. Shirzad E. Accurate and fast model for single rotor double stator interior permanent magnet brushless synchronous machine with spoke-type structure at no-Load. 2023.
43. Shirzad E. Control of Energy and Torque for switched Reluctance Machine. 2024.